

# Motion of Cometary Dust

Marco Fulle

*Istituto Nazionale di Astrofisica–Osservatorio Astronomico di Trieste*

---

On timescales of days to months, the motion of cometary dust is mainly affected by solar radiation pressure, which determines dust dynamics according to the particle-scattering cross-section. Within this scenario, the motion of the dust creates structures referred to as dust tails. Tail photometry, depending on the dust cross-section, allows us to infer from model runs the best available outputs to describe fundamental dust parameters: mass loss rate, ejection velocity from the coma, and size distribution. Only models that incorporate these parameters, each strictly linked to all the others, can provide self-consistent estimates for each of them. After many applications of available tail models, we must conclude that comets release dust with mass dominated by the largest ejected boulders. Moreover, an unexpected prediction can be made: The coma brightness may be dominated by light scattered by meter-sized boulders. This prediction, if confirmed by future observations, will require substantial revisions of most of the dust coma models in use today, all of which are based on the common assumption that coma light comes from grains with sizes close to the observation wavelength.

## 1. HISTORICAL OVERVIEW

While ices sublime on the nucleus surface, the dust embedded in them is freed and dragged out by the expanding gas. The dust motion then depends on the three-dimensional nucleus topography and on the complex three-dimensional gas-dust interaction that takes place close to the nucleus surface. Information on such processes has never been available to modelers. Dust coma shapes depend heavily on the details of these boundary conditions, and coma models cannot disentangle the effect of dust parameters on coma shapes from those due to the unknown boundary conditions. On the contrary, dust tails are usually structureless, suggesting that the dust has lost the memory of the details of the boundary conditions. Moreover, solar radiation pressure acts like a mass spectrometer, putting dust particles of different masses in different space positions: This allows models to evaluate how dust parameters affect tail shapes, making tail models powerful tools to describe dust in comets.

A dust tail is a broad structure that originates from the comet head and can reach lengths on the order of  $10^4$  km in most cases and up to  $10^8$  km in the most spectacular cases (Plate 16). When we consider the comet orbital path and the straight line going from the Sun to the comet nucleus (the radius vector), we divide the comet orbital plane in four sectors (Fig. 1). All cometary tails lie in the sector outside the comet orbit and behind the comet nucleus. When we project these four sectors of the comet orbital plane onto the sky, they may be strongly deformed by the observation perspective, especially when Earth is close to the comet orbital plane. In these latter cases, the sector where tails may be seen can be a complete sky halfplane and the appearance of a perspective antitail is then possible, which although seen to roughly point to the Sun, is always external to the comet orbit. A few years ago, *Pansecchi et al.* (1987) discovered

a particular type of antitails (anti-neck-lines) that lie in the sector opposite that where most tails are possible. These are much shorter than usual tails, not exceeding  $10^6$  km in length (section 7.1).

The first tail model that fit the observations well was developed by Friedrich W. Bessel (1784–1846) and later refined by Fjodor A. Bredichin (1831–1904). Bredichin introduced the notion of synchrones and syndynes (Fig. 1). Both authors assumed that a repulsive force, inversely proportional to the squared Sun-comet distance, was acting on the material composing the tails. According to this hypothesis, the tail particle is subjected to a total force equal to the solar gravity times a factor  $\mu$  characterizing the tail particle. When  $\mu = 0$ , the tail particle assumes a uniform straight motion. When  $\mu < 0$ , the tail particle moves on a hyperbola with the convexity directed toward the Sun. When  $0 < \mu < 1$ , the tail particle behaves as if the Sun were lighter, so that its motion is slower than that of the comet nucleus and its orbit is external relative to that of the comet nucleus. This model explained why cometary tails always lie in the comet orbital plane sector outside of the comet orbit and behind the comet nucleus. Svante Arrhenius (1859–1927) proposed the solar radiation pressure as a candidate for Bessel's repulsive force. The computations of Karl Schwarzschild (1873–1916) and Peter J. W. Debye (1884–1966) established that the  $\beta = 1 - \mu$  parameter is inversely proportional to the diameter of the dust particle (assuming it to be a sphere) and equal to 1 for dust diameters close to  $1 \mu\text{m}$ .

Let us consider the comet nucleus moving along its orbit and ejecting dust particles with exactly zero ejection velocity. Particles all ejected at the same time and characterized by any  $\mu$  value will be distributed at a later observation time on a line referred to as “synchrones.” Changing the ejection time, we obtain a family of synchrones, each characterized

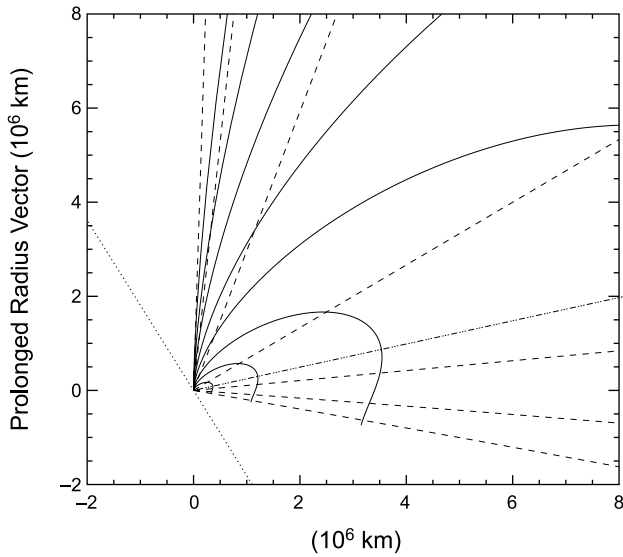


**Fig. 1.** Synchrone-syndyne network for Comet Hale-Bopp 1995O1 on 3 January 1998, when a neck-line was observed during the Earth crossing of the comet orbital plane (Fig. 2). The Sun was located exactly toward the  $-y$  direction and the phase angle of the comet at the observation was  $\phi = 14.4^\circ$ . The image plane corresponds to the comet orbital plane; the Earth direction is toward the bottom right, forming an angle  $\phi$  with the  $-y$  axis. The dotted line is the comet elliptical orbit, which, together with the  $y$  axis, divides the plane in the four sectors discussed in section 1. The continuous lines are syndynes characterized by the parameter  $\beta = 1 - \mu = 1, 0.3, 0.1, 0.03, 0.01, 0.003, 0.001, \text{ and } 0.0003$ , rotating clockwise from that closest to the  $+y$  direction, respectively. The dashed lines are synchrones characterized by the ejection times 250, 200, 100, 0,  $-100$ ,  $-200$ , and  $-300$  d with respect to perihelion, rotating clockwise from the closest one to the  $+y$  direction respectively. The three-dotted-and-dashed line is the neck-line axis, approximately corresponding to the synchrone ejected 43.8 d before perihelion. Because of the Earth position, it is evident that the neck-line was observed as a spike pointing toward the antisolar direction (Fig. 2); its prolongation in the  $-x$  direction was observed as a bright spikelike real antitail (Fig. 2).

by its ejection time. Synchrones can be approximated by radial lines, all diverging from the comet nucleus. Conversely, particles characterized by the same  $\mu$  value ejected at any time will be distributed at a later observation time on a line referred to as “syndyne.” Changing the  $\mu$  value, we obtain a family of syndynes, each characterized by its  $\mu$  value. Syndynes can be approximated by spirals tangent to the prolonged radius vector, the Sun-comet nucleus vector. In this model, only one synchrone and one syndyne pass in each point of the tail. It is thus possible to derive the ejection time and the  $\mu$  value at each point of the tail. The synchrone-syndyne model predicts that dust tails are two-dimensional structures lying in the comet orbital plane. Tail observations made when Earth crosses the comet orbital plane (Pansecchi *et al.*, 1987) have shown that dust tails are thick, i.e., three-dimensional structures.

## 2. DUST TAILS: PHOTOMETRIC THEORY

The dust dynamics depend on the  $\beta = 1 - \mu$  parameter

$$\beta = 1 - \mu = \frac{3E_{\odot}Q_{pr}}{8\pi cGM_{\odot}\rho_d d} = \frac{C_{pr}Q_{pr}}{\rho_d d} \quad (1)$$

where  $E_{\odot}$  is the mean solar radiation,  $c$  the light speed,  $Q_{pr}$  the scattering efficiency for radiation pressure,  $G$  the gravitational constant,  $M_{\odot}$  the solar mass,  $\rho_d$  the dust bulk density and  $d$  the diameter of the dust grains, assumed here to be spherical in shape. Here we use the terms dust grain or dust particle to refer to every solid object that escapes a comet nucleus. The resulting value of  $C_{pr} = 1.19 \times 10^{-3} \text{ kg m}^{-2}$ . For the  $\beta$  values most common in dust tails,  $d \gg 1 \mu\text{m}$  and  $Q_{pr} \approx 1$  (Burns *et al.*, 1979), so that the most uncertain parameter is the dust bulk density. As a consequence, it is convenient to express all size-dependent quantities as functions of  $\rho_d d$ . The flux of photons  $I$  (measured in  $\text{Jy sr}^{-1}$ ) received from a dust tail is

$$I(x, y) = BD(x, y) = B \int_{-\infty}^{t_0} \int_0^{\infty} H(x, y, t, 1 - \mu) \dot{N}(t) \sigma(t, 1 - \mu) dt d(1 - \mu) \quad (2)$$

where  $x, y$  are the sky coordinates,  $H$  the sky surface density of dust grains coming from dust tail models,  $\dot{N}(t)$  the dust number loss rate,  $t_0$  the observation time,  $\sigma$  the cross-section of a grain,  $B$  the flux of photons in thermal or optical bandwidths (measured in  $\text{Jy sr}^{-1}$ ) received from a grain of unit cross-section, and  $D$  the dimensionless sky surface density weighted by the dust cross-section observed in the tail: If we are observing optical fluxes, then we are dealing with scattering cross-sections; if we are observing IR fluxes coming from grains with sizes much larger than IR wavelengths, then we are dealing with emitting cross-sections. Since we have

$$\sigma(d) = \frac{\pi}{4} d^2 = \frac{\pi}{4} \frac{(\rho_d d)^2}{\rho_d^2} \quad (3)$$

$$\dot{M}(d) = \dot{N} \frac{\pi}{6} \rho_d \frac{(\rho_d d)^3}{\rho_d^3} \quad (4)$$

the relation between the dust mass loss rate  $\dot{M}$  and the flux  $I$  received from the tail is independent of  $\rho_d$

$$I(x, y) = \frac{3}{2} B \int_{-\infty}^{t_0} \int_0^{\infty} H(x, y, t, 1 - \mu) \dot{M}(t, 1 - \mu) \frac{(\rho_d d)^2}{(\rho_d d)^3} dt d(1 - \mu) \quad (5)$$

which makes dust tail models a powerful tool to infer the

mass loss rate of cometary dust. Equation (5) shows that the relationship between dust mass loss rate and tail brightness depends on the second and third moments of the differential dust size distribution (DSD). Since the dust dynamics depend on the  $\beta = 1 - \mu$  quantity, it is convenient to express the DSD in terms of  $(\rho_d d)$  weighted by the dust cross-section observed in the tail. Thus, we define the dimensionless “ $\beta$ -distribution”

$$f(t, 1 - \mu)d(1 - \mu) = \frac{(\rho_d d)^2 g(t, \rho_d d)d(\rho_d d)}{\int_0^\infty (\rho_d d)^2 g(t, \rho_d d)d(\rho_d d)} \quad (6)$$

$$g(t, \rho_d d)d(\rho_d d) = k(1 - \mu)^2 f(t, 1 - \mu)d(1 - \mu) \quad (7)$$

where  $k$  is a dimensionless constant depending on the quantity  $B$  defined in equation (2). If the DSD  $g(t, \rho_d d)$  is a power law vs.  $(\rho_d d)$  with index  $\alpha$ , then  $f(t, 1 - \mu)$  is a power law vs.  $(1 - \mu)$  with index  $-\alpha - 4$ . Dust tail models provide the quantity  $F(t, 1 - \mu)$ , which is expressed in  $\text{m}^2 \text{s}^{-1}$

$$F(t, 1 - \mu) = \left[ \frac{C_{\text{pr}} Q_{\text{pr}}}{\rho_d} \right]^2 \dot{N}(t) f(t, 1 - \mu) \quad (8)$$

so that the dust mass loss rate given by equation (4) becomes

$$\dot{M}(t) = \frac{\pi}{6} k C_{\text{pr}} Q_{\text{pr}} \int_0^\infty \frac{F(t, 1 - \mu)}{1 - \mu} d(1 - \mu) \quad (9)$$

Values of dimensionless quantity  $k$  depend on the actual techniques used to observe the dust tail. In the case of optical photographic or CCD data, it becomes

$$k = \frac{4}{A_p(\phi)} \left[ \frac{\gamma r}{1 \text{ AU}} \right]^2 \frac{10^{0.4[m_\odot - m(x, y)]}}{D(x, y)} \quad (10)$$

where  $\gamma = 206265$  arcsec;  $r$  the Sun-comet distance at observation;  $m(x, y)$  the dust tail brightness expressed in mag arcsec $^{-2}$ ;  $m_\odot$  the Sun magnitude in the bandwidth of tail observations;  $D(x, y)$  the dimensionless tail brightness defined in equation (2); and  $A_p(\phi)$  is the geometric albedo times the phase function at observation [an isotropic body diffusing all the received radiation uniformly in all directions has  $A_p = \frac{1}{4}$  (Hanner et al., 1981)]. CCD data provide much better observational constraints to models, because they have a well-calibrated photometric response, unlike photographic plates. Moreover, the much higher sensitivity of CCDs allows us to use interferential filters to avoid emissions from ions and gases, which usually pollute the wide bandwidths (e.g., Johnson filters) used in astrophotography. However, CCD data also provide dust mass loss rates that are dependent on the poorly known dust albedo. Conversely, in the case of ther-

mal IR or millimeter data

$$k = \frac{4S_v(x, y, T)}{\pi D(x, y)B_v(T)} \quad (11)$$

so that  $k$  is now independent of the dust albedo, depending only on the dust temperature  $T$ , usually much better known than the albedo. Here,  $B_v(T)$  is the Planck function at temperature  $T$  and  $S_v(x, y, T)$  is the flux received from a dust tail in a thermal IR or millimeter wavelength. If the dust grains have very aspherical shapes, with very different cross-sections along each space coordinate (e.g., noodles, long cylinders or flat disks), then it becomes impossible to compute any dust dynamics (Crifo and Rodionov, 1999). If dust grains are not spherical but still compact, then the numerical values of  $C_{\text{pr}}$  and  $k$  change, while equations (1), (2), (6), (7), (8), and (9) remain identical (where now  $d$  is the mean grain size), along with equations (3), (4), and (5) after we change only the factors  $\frac{\pi}{4}$ ,  $\frac{\pi}{6}$ , and  $\frac{3}{2}$  respectively. Therefore, thermal IR or millimeter tail data provide the most reliable information on dust mass loss rates and DSDs in comets. In fact, the outputs of IR tail models are completely independent of the dust shape (provided the grains are compact), bulk density, and albedo (i.e., the most uncertain parameters in cometary dust modeling). Moreover, parallel IR and optical observations made at the same time can provide unique estimates of the size and time dependency of the dust albedo.

### 3. TWO-DIMENSIONAL MODELS

If we assume that dust, after having been dragged out by the expanding gas, is ejected from the coma at zero velocity with respect to the nucleus, then the resulting two-dimensional model depends only on the quantity  $F$  given by equation (8). Within this model, the dust tail is a thin dust layer lying in the comet orbital plane. The dust tail brightness  $D$  is simply proportional to  $F$  multiplied by the determinant of the Jacobian between the  $(x, y)$  frame and the syndyne-synchrone network defined in section 1. Then equation (5) is directly invertible, easily providing the quantity  $F$ , from which we can infer the dust mass loss rate by equation (9) and the DSD by means of the normalization of  $F$  vs.  $\beta$  and then by equation (7). Following such a direct approach, the DSD of short-period Comets 2P/Encke and 6P/d'Arrest was obtained (Sekanina and Schuster, 1978). The DSD power index was always  $\alpha < -4$ . In this case, both the brightness and the mass mainly depend on the micrometer-sized grains observed in the tail. If  $\alpha > -3$ , both the mass and brightness depend on the largest ejected grains. Brightness and mass become decoupled if  $-4 < \alpha < -3$ , in which case the dust mass depends on the largest ejected grains, while the brightness depends on the micrometer-sized grains.

Since the observed brightness fixes the number of micrometer-sized grains observed in the comet if  $\alpha < -3$ , the DSD index in practice only affects the number of unob-

TABLE 1. Dust size distributions in comets.

Comet	$\beta_{\min}$	$\beta_{\max}$	$\alpha(t)$	$\alpha_m$
2P/Encke	$6 \times 10^{-6}$	0.02	$-4.8 < \alpha < -2.8$	$-3.6 \pm 0.3$
6P/d'Arrest	$1 \times 10^{-5}$	0.06	$-5.0 < \alpha < -3.5$	$-3.8 \pm 0.1$
10P/Tempel2	$2 \times 10^{-5}$	0.03	$-4.8 < \alpha < -3.4$	
26P/Grigg-Skjellerup	$6 \times 10^{-5}$	0.06	$-4.0 < \alpha < -3.0$	
29P/SW1	$4 \times 10^{-5}$	0.2	$-4.0 < \alpha < -3.0$	$-3.3 \pm 0.3$
46P/Wirtanen	$1 \times 10^{-4}$	0.2	$-4.1 < \alpha < -3.0$	
65P/Gunn	$1 \times 10^{-4}$	0.2	$-4.3 < \alpha < -3.0$	
67P/Churyumov-Gerasimenko	$6 \times 10^{-6}$	0.03	$-5.5 < \alpha < -3.2$	$-3.4 \pm 0.2$
P/Swift-Tuttle	$6 \times 10^{-5}$	0.2	$-5.0 < \alpha < -3.0$	$-3.3 \pm 0.2$
2060 Chiron	$2 \times 10^{-4}$	1.0	$-4.5 < \alpha < -3.0$	$-3.2 \pm 0.1$
Seki-Lines 1962III	$1 \times 10^{-4}$	0.1	$-5.0 < \alpha < -4.0$	$-4.1 \pm 0.6$
Kohoutek 1973XII	$1 \times 10^{-4}$	0.2	$-5.0 < \alpha < -3.0$	$-3.3 \pm 0.4$
Wilson 1987VII	$2 \times 10^{-5}$	0.1	$-3.8 < \alpha < -2.8$	$-3.0 \pm 0.1$
Bradfield 1987XXIX	$1 \times 10^{-4}$	0.6	$-4.2 < \alpha < -3.0$	$-3.2 \pm 0.2$
Liller 1988V	$1 \times 10^{-5}$	0.06	$-4.3 < \alpha < -3.3$	$-3.5 \pm 0.2$
Austin 1990V	$1 \times 10^{-5}$	0.1	$-4.5 < \alpha < -2.8$	$-3.0 \pm 0.2$
Levy 1990XX	$6 \times 10^{-5}$	0.4	$-5.0 < \alpha < -3.0$	$-3.2 \pm 0.1$
Hyakutake 1996B2	$4 \times 10^{-4}$	1.0	$-4.7 < \alpha < -3.0$	$-3.6 \pm 0.2$
Hale-Bopp 1995O1	$2 \times 10^{-3}$	1.0	$-4.2 < \alpha < -3.2$	$-3.6 \pm 0.1$

Time-dependent [ $\alpha(t)$ ] and time-averaged ( $\alpha_m$ ) DSD power index evaluated for various comets within a  $\beta$  range (defined by  $\beta_{\min}$  and  $\beta_{\max}$ ) by means of the inverse tail model (adapted from *Fulle*, 1999).

served large grains, which may dominate the ejected mass if  $\alpha > -4$  as well. Therefore, *Sekanina and Schuster* (1978) correctly concluded that the index they found ( $\alpha = -4.2$ ) implied that the number of ejected large grains was negligible, and this assumption was adopted to design the European Space Agency's *Giotto* mission to 1P/Halley. The impact of *Giotto* with a grain of 1 g at the flyby implied that the actual probability of such an impact was underestimated by at least a factor of 100. Since the size ratio between 1-g grains and those dominating the brightness of Comets 2P/Encke and 6P/d'Arrest was  $10^4$ , the real  $\alpha$  value should have been  $\alpha > -3.7$ . We should conclude either that the dust population of 1P/Halley is very different from that of 2P/Encke or 6P/d'Arrest, or that the two-dimensional model has intrinsic severe shortcomings.

Observations when Earth crosses the comet orbital plane, and hydrodynamic models describing the dust-gas interaction in the coma, both point out that the assumption of zero dust ejection velocity is nonphysical. Let us recall that this approximation is also useless for the so-called perspective antitails, which are sometimes composed of dust released at very large heliocentric distances. In this latter case, the likely very low dust velocity is balanced by the very long time interval existing between ejection of the dust and observation. Since the thickness of the tail is roughly given by such a time interval times the dust velocity, it is impossible to obtain a dust tail that can be well approximated by a two-dimensional model based on synchrones and syndynes. This is also true for apparently thin antitails observed, e.g., in Comet Arend-Roland 1957III: *Kimura and Liu* (1977) have

shown that the correct explanation for these spikes requires a model more elaborate than the two-dimensional syndyne-synchrone model.

After we have shown that the two-dimensional tail model has no physical basis, we must also show that the predictions of this two-dimensional model are systematically different from those of a correct three-dimensional model applied to the same data. This was done, and in fact the DSD power index resulted in  $\alpha \approx -3.7$  for Comet 2P/Encke and Comet 6P/d'Arrest (*Fulle*, 1990) (Table 1). The fact that the dust mass in 2P/Encke is strongly dominated by the largest ejected grains was further confirmed by applying the same three-dimensional model to independent IR thermal data provided by the ISO probe [ $\alpha = -3.2$ ; *Epifani et al.* (2001)]. These results show that two-dimensional models and all related outputs should be ignored in the future, as they are unable to provide useful constraints on the derived cometary dust properties.

#### 4. THREE-DIMENSIONAL MODELS

*Finson and Probststein* (1968) showed that the unrealistic two-dimensional synchrone-syndyne models can be converted into realistic three-dimensional models when we associate a synchronic tube to each synchrone, whose width is given by the dust ejection velocity at the synchrone time, or a syndynamic tube to each syndyne, whose width is given by the dust ejection velocity of the syndyne  $\beta$  value. In the synchronic approach, they analytically computed the dimensionless sky surface density of a synchronic tube

$$dD(x, y, t) = \frac{F(t, 1 - \mu)dt}{2(t_0 - t)v(t, 1 - \mu) \frac{ds}{d(1 - \mu)}} \quad (12)$$

so that the brightness of the whole tail is simply proportional to the numerical time integral of equation (12). Equation (12) is derived from an analytical integration that is correct if the following condition (named by Finson and Probststein, although quite improperly, hypersonic) is satisfied

$$\frac{ds}{d(1 - \mu)} \gg \frac{(t_0 - t)v(t, 1 - \mu)}{1 - \mu} \quad (13)$$

This usually happens in the outermost dust tail only. In equations (12) and (13),  $s$  is the parametric coordinate along the synchronic and  $v(t, 1 - \mu)$  the dust ejection velocity. In equation (12), the synchronic (or syndynamic) tubes are assumed to have circular sections, because the dust tail is supposedly built up by dust shells that keep their spherical expanding shape over time if significant tidal effects due to the solar gravity are neglected. The spherical shell assumption implies that the dust ejection is isotropic, another strong approximation. When the numerical integration of equation (12) is performed, the fit of the tail brightness data is performed by trial and error, so we cannot ensure the uniqueness of the obtained dust loss rate, ejection velocity, and size distribution. All these approximations make the Finson-Probststein model a first-order model that is unable to give realistic estimates of the dust parameters. *Fulle* (1987, 1989) developed an inverse Monte Carlo dust tail model by taking into account all the improvements introduced by *Kimura and Liu* (1977) and avoiding all the limitations and approximations of the Finson-Probststein model: (1) It computes the rigorous heliocentric Keplerian orbits of millions of sampling dust grains, so that the spherical shell approximation is avoided. (2) It performs both the size and time integral by means of numerical methods, so that the condition imposed by equation (13) is avoided. In this way, it can fit not only the external tail, but also the inner one, as close as desired to the dust coma, where the largest grains usually reside. (3) It takes into account anisotropic dust ejections. (4) It provides for each dust size a dust ejection velocity from the coma that is the mean value of a wide velocity distribution (*Fulle*, 1992); this is consistent with the predictions of three-dimensional dust-gas interaction models in the inner coma (*Crifo and Rodionov*, 1999). (5) It avoids the trial-and-error procedure typical of the original Finson-Probststein model, by means of an inverse ill-posed problem theory. In this way, the uniqueness of the results (impossible to establish in the original Finson-Probststein approach) is recovered in the least-squares-fit sense.

Within the inverse Monte Carlo dust tail model, the dust ejection velocity, loss rate, and size distribution are obtained through minimization of the function

$$(HF - D)^2 + (RF)^2 = \min \quad (14)$$

where  $H$  is the kernel matrix provided by the dust tail model defined in equation (2),  $F$  (solution vector defined in equation (8)) is the output of the inversion of equation (14),  $D$  is the dust tail dimensionless sky surface density (data vector defined in equation (2)), and  $R$  is a regularizing constraint to drop noise and negative values in solution  $F$ . The inverse Monte Carlo approach was applied to tens of dust tails: The results regarding the DSD (Table 1) and the dust mass loss rate will be discussed in sections 5 and 6. In general, dust ejection velocities show time and size dependencies more complex than predicted by one-dimensional coma models of dust-gas interaction. In particular, the velocity of large grains relative to that of small ones seems higher than expected. This result was confirmed by independent tail models that left free such a parameter (*Waniak*, 1992, 1994). This points out that dust-gas interaction must be treated by three-dimensional coma models to predict reliable dust ejection velocities. In most cases the accuracy of the fit of the observed tail brightness did not change after varying the assumed dust ejection anisotropy. This fact confirms that tail shapes have lost memory of the details of the unknown boundary conditions of the three-dimensional gas drag occurring in the inner coma.

Other Monte Carlo dust tail models were developed that followed other approaches (e.g., *Waniak*, 1994; *Lisse et al.*, 1998). Equation (2) allows us to fit more details of the input tail data by means of a time- and size-dependent dust-scattering cross-section [i.e., by  $f(t, 1 - \mu)$ ]. If the DSD is assumed to be time-independent to stabilize the model outputs, then it may become impossible to perfectly fit the tail data. The assumption of a time-independent DSD is commonly made: *Lisse et al.* (1998) analyzed dust tails at millimeter wavelengths (COBE satellite data) with a poor spatial resolution (20 arcmin), so that rough assumptions on DSD [ $f(1 - \mu) = (1 - \mu)^{-1}$  implying  $\alpha = -3$ ] allowed them to fit the input images. *Waniak* (1994), adopting a constant  $\alpha \approx -3$ , improved the tail fit of Comet Wilson 1987VII by means of a detailed dust ejection pattern. However, the fact that this pattern ejects dust mainly on the nucleus nightside may indicate that temporal variations of the DSD are likely responsible for the shape of dust tails.

## 5. DUST SIZE DISTRIBUTION IN COMETS

The dust size distribution (DSD) plays a crucial role when we describe the behavior of dust particles in comets. For instance, it is widely believed that in dust comae we mainly see grains with sizes close to the observation wavelength. It is easy to conclude (see equation (15) in section 6.1) that the coma brightness depends on the size of the largest ejected particle if  $\alpha > u - 3$ , where  $u$  is the power index vs.  $(\rho_d d)$  of the dust velocity. The assumptions ( $\alpha = -3.0$  and  $u = -0.5$ ) made by *Lisse et al.* (1998) imply that, if  $\alpha > -3.5$ , then the dust coma brightness at optical wavelengths is dominated by the contribution from the largest ejected boulders. Since dynamical models in comae of micrometer-sized grains or of meter-sized boulders are quite

different, it is crucial to understand which dust is observed. The total mass of the dust depends on the size of the largest or the smallest ejected grains according to the actual DSD: It is fundamental to define the size range to which the published results are related, although this is usually not done. For usual  $\alpha > -4$ , the dust mass diverges if we allow it to reach the nucleus size. It is impossible to compare dust masses without knowing which largest boulder size they refer to.

We applied the inverse tail model to tens of cometary dust tails, which always resulted in dust grains ranging in size between 1  $\mu\text{m}$  and about 1 cm (Table 1). The DSD often showed large temporal changes: Since most output instabilities affect the DSD time-dependency, in section 6.2 we will pay special attention to testing the correctness of this model output. The time-averaged DSD is much more stable: In almost all comets it was characterized by an index  $\alpha \approx -3.5$ . This index is typical of a population of collisionally evolved bodies (*Dohnanyi, 1972*): Should this index value be further confirmed, it would suggest that we do not observe in comets the pristine dust population of the presolar nebula. The  $\alpha = -3.5$  value is the most critical for models aimed to fit the brightness and/or the time evolution of coma features, like jets or spirals. In fact, if  $\alpha = -3.5$  and  $u = -0.5$  [this value is provided by one-dimensional models of dust-gas interaction at  $d > 1 \mu\text{m}$  (*Crifo, 1991*)], then a correct computation of the brightness of every feature observed in a dust coma must take into account grains of every size, from submicrometers up to tens of meters. Also, these large boulders, when present in a dust coma, provide a significant fraction of the observed brightness if  $\alpha = -3.5$  and  $u = -0.5$ . While it is possible to come up with a theory of dust tails that can separate the dependency of the numerous dust parameters required to interpret the data, this becomes impossible in models of dust comae.

An important dataset providing DSD in comets is given by the only available *in situ* data we have so far: the results of the DID experiment on *Giotto* (*McDonnell et al., 1991*) during the 1P/Halley flyby. The power index fitting the DSD at the nucleus, traced back from the DID fluence in terms of purely radial expansion, is  $\alpha \approx -3.7$  for dust masses between  $10^{-14}$  and  $10^{-3}$  kg. This slope is also consistent with the impact of the 1-g grain that damaged the probe itself. This example shows how models crucially affect the interpretation of the dust data. The fit of the same data by means of a rigorous dust dynamical model changed the results completely (*Fulle et al., 2000*). The DID fluence was found to be consistent with any  $-2.5 < \alpha < -3.0$ , strongly supporting the possibility considered by *Lisse et al. (1998)*, that the coma brightness is dominated by meter-sized boulders. The same model also inferred the dust-to-gas ratio ( $3 < \text{DGR} < 40$  for dust masses up to 1 g) and the dust geometric albedo ( $0.01 < A_p < 0.15$ ) by means of the Optical Probing Experiment data (*Levasseur-Regourd et al., 1999*), with a correlation between  $A_p$  and  $\rho_d$  ( $\rho_d = 2500 A_p \text{ kg m}^{-3}$ ). Tail models and DID experiments agree with these conclusions: (1)  $\alpha \gg -4$ ; (2) the dust mass (we cannot exclude the light

flux too) depends on the size of the largest ejected boulders; and (3) the DGR is  $>1$  for particle sizes larger than 1 cm.

All available results confirm that the mass of dust ejected from comets is dominated by the largest boulders. Radar observations (*Harmon et al., 1989*) operating at centimeter wavelengths and coma observations at millimeter wavelengths provide first-quality constraints to this conclusion, because they directly observe grains close in size to the observation wavelength if  $\alpha < -3.5$ , while they observe dust larger than the observation wavelength if  $\alpha \gg -3.5$ . Observations of P/Swift-Tuttle (*Jewitt, 1996*) and C/Hyakutake 1996B2 (*Jewitt and Matthews, 1997*) at millimeter wavelengths provided loss mass rates 7 and 10 times higher, respectively, than predicted by tail models (*Fulle et al., 1994, 1997*). Observations at millimeter wavelengths therefore suggest that  $\alpha$  was higher than  $\alpha = -3.3$  and  $\alpha = -3.6$  respectively (Table 1). We must conclude that the dust coma brightness of these two comets was dominated at all observation wavelengths by the largest ejected boulders if index  $u$  is  $-0.5$  (this value is predicted by one-dimensional dust-gas-drag models in the inner coma).

Is a power law a proper function to describe the DSD? This assumption is usually adopted by direct tail modelers only (e.g., *Lisse et al., 1998*). Inverse tail models do not assume that the DSD is a power law; they leave it completely free, sampling the DSD in  $\beta$ -bins. Then, the output describing the DSD is fit by a power law to offer an easily understandable DSD. Sometimes, the direct  $f(t, 1 - \mu)$  output was provided (e.g., *Fulle et al., 1998*). In any case, no DSD data are determined accurately enough to require more than a power law in order to fit them: A power-law DSD is consistent with the DID fluence measured at 1P/Halley, which is not a power law of the dust size (*Fulle et al., 2000*). Other functions were suggested to describe the DSD of cometary dust. *Hanner (1984)* proposed a more complex function, which becomes a simple power law at the largest sizes ( $d > 1 \text{ mm}$ ), and drops rapidly to zero at submicrometer grains. This function was used to fit the IR photometry and spectra of comets. These observations are unable to detect submicrometer grains, and thereby provide a typical example of “absence of evidence” interpreted as “evidence of absence.” In fact, *Giotto* showed that in 1P/Halley, submicrometer grains were more abundant than larger ones (*McDonnell et al., 1991*). This is probably true for all comets: Many authors pointed out that every DSD discussed in this review is consistent with all available IR spectra (*Crifo, 1987; Greenberg and Li, 1999*). Dust tail models and *in situ* data provide much better constraints to the DSD than IR spectra, and show that a power law defined within a precise size interval is the best approach for describing the DSD in comets, avoiding misleading conclusions suggested by more complex and underconstrained size functions.

It would seem obvious that a comet is defined as “dusty” according to its dust-to-gas ratio. In other words, we would like to find that the higher the index  $\alpha$ , the higher the released dust mass, and the more “dusty” the comet. This is not the case. Usually, a comet is said to be “dusty” when

spectral features in its IR spectrum or high polarization are observed. However, it is hard to relate these observed characteristics to the actual released dust mass. In particular, when the silicate feature at 10  $\mu\text{m}$  is strong (*Lisse, 2002*), or when the highest polarization is higher than 20% (*Levasseur-Regourd et al., 1996*), the comet is then recognized as “dusty.” Both these features refer to the actual population of micrometer-sized grains, which we have seen to be a minor component of the total released mass. If the DSD has a turning point at some size larger than 10  $\mu\text{m}$ , where at smaller sizes  $\alpha$  becomes larger than 1P/Halley’s index, then the relative production of micrometer-sized grains drops compared to 1P/Halley. In this case, the comet is defined as less “dusty” than 1P/Halley, even though its  $\alpha$  from millimeters to meters may be much higher, with a much higher released dust mass.

## 6. CONSTRAINTS TO THE OUTPUTS OF THREE-DIMENSIONAL TAIL MODELS

### 6.1. Dust Coma Equivalent Size $A_{fp}$

The model outputs  $F$  and  $v$  can be compared to the observed dust coma brightness. This is usually measured by means of the  $A_{fp}$  quantity (*A’Hearn et al., 1984*)

$$A_{fp}(t) = 2\pi \left[ \frac{\gamma r}{1 \text{ AU}} \right]^2 \frac{10^{0.4[m_{\odot} - m(x,y)]}}{D(x,y)} \int_0^{\infty} \frac{F(t, 1-\mu)}{v(t, 1-\mu)} d(1-\mu) \quad (15)$$

where all the quantities are defined in section 2.  $A_{fp}$  is related to the total dust cross-section  $\Sigma$  observed inside the observation field of radius  $\rho$  (in meters projected at the comet) centered exactly on the comet nucleus

$$\Sigma = \frac{\pi\rho}{4A_p(\phi)} A_{fp} \quad (16)$$

We note that equation (15) is completely parameter-free: Given the outputs  $F$  and  $v$  of the tail model, there is no way to adjust the tail model to fit the observed  $A_{fp}$  values. However, the integral of equation (15) can be computed on a finite  $\beta$  range, while  $A_{fp}$  is measured observing all the ejected dust sizes in the dust coma. Therefore, if the size range adopted to compute equation (15) loses dust sizes reflecting a significant light fraction in the coma, then tail models can provide only a lower limit of the actually observed  $A_{fp}$ . In any case,  $A_{fp}$  computed by means of equation (15) was always consistent with that observed (*Fulle et al., 1998; Fulle, 2000*).

Equations (9) and (15) point out that  $A_{fp}$  has little to do with the dust mass loss rate. Nevertheless, it is commonly referred to as the dust loss rate, despite its dimensions, and

is commonly related to the water loss rate to obtain incorrect (at least from a physical point of view) dimensional ratios. It is obvious that comets with a higher  $A_{fp}$  can eject less dust mass: This depends on the DSD and dust velocity. Moreover, the time evolution of  $A_{fp}$  can be unrelated to the loss rate time evolution, depending on time changes of the DSD and velocity.  $A_{fp}$  is a high-quality constraint for physical models of comae and tails, but nothing more.

### 6.2. Dust Size Distribution Time Variability

So far, only inverse dust tail models take into account the possibility that dust is ejected from the cometary nucleus with a DSD that may change in time. Despite the high or low probability that this really happens in comets, it is surprising that most models describing dust in comets adopt time-independent DSDs, because most papers on cometary dust invoke dust fragmentation to explain the observations. It is obvious that dust fragmentation implies a time evolution of the DSD, and a model that takes into account a time-dependent DSD is more general than others that only take dust fragmentation into account. So far, no consistent models of dust fragmentation were developed (*Crifo, 1995*). *Combi* (1994) developed a direct dust tail model with fragmentation that was based on consistent fits of both the dust coma and tail. Many tests performed by means of the inverse tail model that adopted numerous  $u$  values showed that such a consistent fit to both the dust coma and the tail simply requires  $-0.5 \ll u < -0.1$ . *Fulle et al.* (1993) showed that dust fragmentation is a possible (not unique) explanation of  $-0.5 \ll u < -0.1$ .

While inverse dust tail models can provide a stable time-averaged DSD, the time-dependent DSD is affected by residual instability. It is not easy to establish if large and systematic changes of the DSD are real or simply due to output instability. The most elegant solution is to find independent observations that suggest systematic changes of the ejected dust population in agreement with the time-evolution of the DSD provided by inverse tail models. These models applied to C/Hyakutake 1996B2 provided an  $\alpha$  value that dropped suddenly from a roughly constant value  $\alpha = -3$  to  $\alpha = -4$  in mid April 1996 (*Fulle et al., 1997*), in perfect agreement with the time evolution of IR spectra; no silicate feature was detected before a strong 10- $\mu\text{m}$  line appeared around mid April (*Mason et al., 1998*). This IR spectral evolution was interpreted in terms of dust fragmentation exposing small silicate cores to the Sun’s radiation; such cores were embedded in large carbonaceous matrices before mid April. The inverse tail model applied both to optical data (*Fulle, 1990*) and to IR thermal data (*Epifani et al., 2001*) collected during two different perihelion passages of Comet 2P/Encke provided a similar drop from  $\alpha = -3$  to  $\alpha = -4$  during the first three weeks after perihelion. This coincidence has already forced us to exclude the possibility that this DSD time-evolution is due to output instability. Moreover, these three weeks match exactly the seasonal night cycle of the most active nucleus hemisphere suggested by *Sekanina*

(1988) to explain the comet photometry and coma shape evolution of 2P/Encke.

## 7. FINE STRUCTURES IN TAILS

### 7.1. Neck-Lines

In several cases, dust tails retain the memory of the dust ejection over more than half the comet orbit; during such long periods of time the tidal effects of solar gravity become significant. *Kimura and Liu (1977)* pointed out that the dust motion is heliocentric, so that at ejection a dust grain can be considered as occurring at the first node of its heliocentric orbit. Every heliocentric orbit has its second node  $180^\circ$  away from the first, where the dust grain orbit must necessarily cross the comet orbit again. When we consider a Finson-Probst dust shell, all these grains, ejected at the same time, will have their second orbital node at approximately the same time, i.e.,  $180^\circ$  away in orbital anomaly, where the spherical dust shell will collapse into a two-dimensional ellipse contained in the comet orbital plane, a shape far removed from a sphere. When we consider a collapsed synchronic tube, we obtain a two-dimensional structure, referred to as the “neck-line” by the discoverers (*Kimura and Liu, 1977*). When Earth crosses the comet orbit, the neck-line appears on the sky as a straight line much brighter than the surrounding dust tail, because all the synchronic tube is collapsed in an infinitesimal sky area (Fig. 2). By means of the neck-line model, *Kimura and Liu* fit perfectly the perspective antitail of Comet Arend Roland 1957III, which appeared as a bright spike many millions of kilometers long and pointing toward the Sun, thus avoiding unrealistic explanations based on dust ejected at zero velocity from the parent coma.

Neck-lines were observed in the Great Comet 1910 I and in Comets Arend-Roland 1957III, Bennett 1970II, 1P/Halley 1986III, Austin 1990V, Levy 1990XX, and Hale-Bopp 1995O1. It must be pointed out that neck-lines can appear only after perihelion of comets orbiting in open orbits (hyperbolic or parabolic), a fact rigorously verified by all the registered apparitions. In the case of periodic comets, dust ejected after perihelion could also form a neck-line before the next perihelion passage. However, this was never observed and seems improbable, because planetary perturbations in short-period comets, and stellar ones in long-period comets, can perturb the dust orbits enough to prevent the formation of a neck-line after periods of many years. Due to the particular perspective conditions, in Comets Arend-Roland and Levy the neck-line appeared as a perspective antitail (it is probable that all observed antitails were in fact neck-lines). In all other comets, it appeared superimposed to the main dust tail as a bright and straight linear feature. Since a neck-line is built up by the collapse of the dust shells into two-dimensional ellipses, the ellipses composed of the largest grains, approximately centered on the comet nucleus, are placed half out of the comet orbit and half inside of it. Due to the long travel time of the dust

grains (usually months), these ellipses may reach huge dimensions, up to  $10^6$  km: When the Earth crossed the orbit plane of Comets Bennett, 1P/Halley, Austin and Hale-Bopp, the half of the ellipse inside the comet orbit was seen as a bright spike pointing to the Sun, which was in fact a real (nonperspective) antitail. Since these real antitails are com-

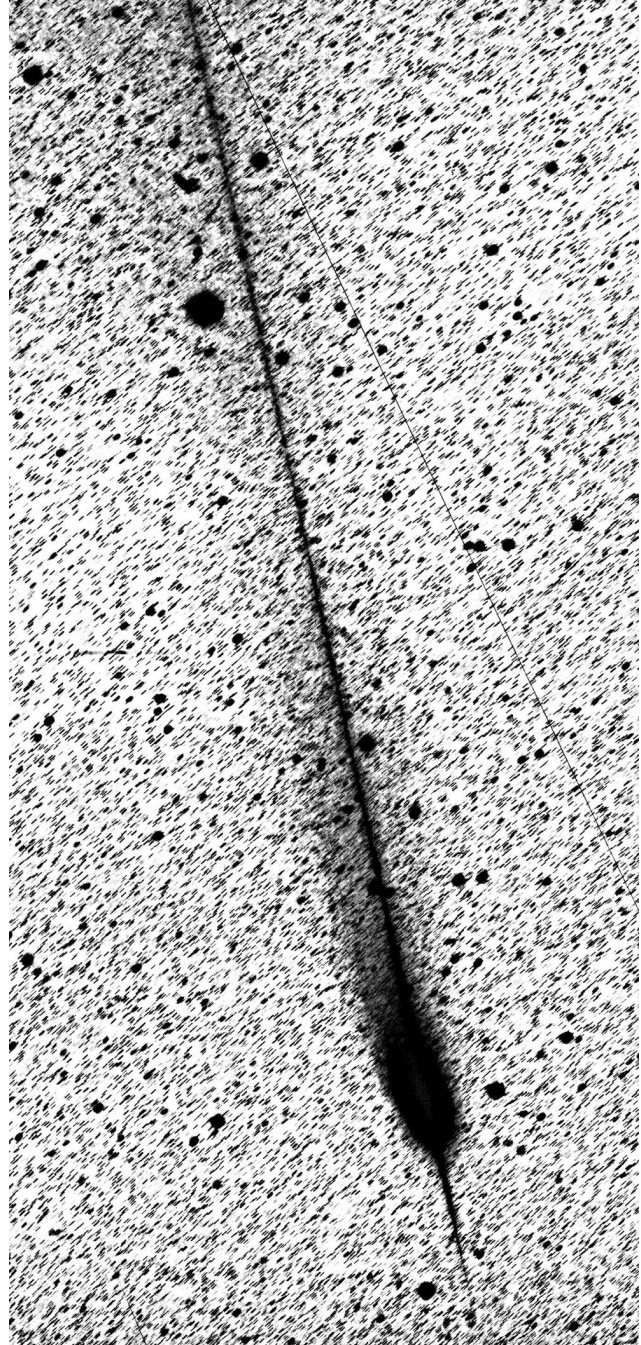


**Fig. 2.** Neck-line observed in Comet Hale-Bopp 1995O1 on 5 January 1998 with the ESO 1-m Schmidt Telescope. The original image was filtered (unsharp masking) to enhance the spike features: the real antitail pointing toward the Sun (bottom) and the neck-line pointing in the opposite direction. ESO Press Photo 05a/98, courtesy of the European Southern Observatory (observer Guido Pizarro).

posed of the largest grains ever observed in dust tails, neck-line observations provide unique information on the ejection velocity and size distribution of grains larger than centimeter-sized.

Fulle and Sedmak (1988) have obtained analytical models of neck-lines, so that the neck-line photometry provides the  $\beta$  distribution and the dust ejection velocity at the ejection time  $t$  of the neck-line. The Keplerian dynamics of the grains in space allow us to compute the geometric neck-line parameters  $a$  and  $b$  (related to the major and minor axes respectively of the ellipses composing the neck-line) and  $s$  (the parametric coordinate along the neck-line axis  $x$ ) defined in Fulle and Sedmak (1988). If the velocity condition

$$v(1 - \mu) \ll (1 - \mu)sa \quad (17)$$

is satisfied, then the dimensionless sky surface density in the neck-line is

$$D(x, y) = \frac{F(t, 1 - \mu)}{sv(1 - \mu)} \left[ 1 + \operatorname{erf} \frac{ax}{v(1 - \mu)} \right] \exp \left[ -\frac{b^2 y^2}{v^2(1 - \mu)} \right] \quad (18)$$

From equation (18), it is apparent that the neck-line width along the  $y$  axis provides a direct measurement of the  $\beta$  dependency of the dust velocity at centimeter sizes. These are the only available direct observations of such a dependency, which is in agreement with the results of three-dimensional inverse dust tail models:  $-0.5 \ll u < -0.1$ . The obtained  $\beta$  distributions confirm that most of the dust mass is released in the form of the largest ejected grains.

### 7.2. Striae

In the brightest comets (e.g., Great Comet 1910I, Comets Mrkos 1957V, West 1976VI, Hale-Bopp 1995O1), the usually structureless dust tail exhibits detailed substructures of two kinds, namely synchronic bands and striae. The synchronic bands are streamers pointing to the comet nucleus, with the axis well fit by synchrones. There is general agreement that they are due to time changes of the dust loss rate or of the DSD, so that the dust cross-section is larger in the synchronic bands than outside. On the contrary, the striae do not point to the comet nucleus (Plate 17), and they are neither fit by synchrones nor by syndynes. There is general agreement that striae are due to instantaneous fragmentation of larger parents, so that the striae are synchrones not originating from the comet nucleus, but from the tail point where the parent was located at the time of fragmentation. This explains well the orientation of the striae, which always point between the comet nucleus and the Sun.

Usually, the interpretations of bands and striae are performed using two-dimensional synchronic-syndyne models, so that the available quantitative results may be affected by significant errors. The dust ejection velocity from the coma

is assumed to be zero, in contradiction with all available information on the dust dynamics. For striae models, in particular, which are very sensitive to the  $\beta$  value of the parent grain, this assumption might significantly affect the results. The  $\beta$  value of the parent is easily obtained by the stria origin in a two-dimensional model, while many different  $\beta$  values are consistent with the stria origin in a three-dimensional model. Sekanina and Farrell (1980) showed that the submicrometer-sized fragments observed in the striae of Comet West 1976VI had a  $\beta$  very similar to their much larger parents. This result would imply that the parents must be very elongated chains of submicrometer-sized grains. However, this also implies that the drag by gas on these chains was correspondingly high (both gas drag and radiation pressure depend on the parent cross-section): These chains must have been ejected from the coma exactly at the gas velocity, so that they would have been diluted over huge  $10^6$ -km-sized shells. The origin of the striae constrains neither the fragmentation time nor the  $\beta$  value of the parent grain.

### 7.3. Sodium Tail

Although spectroscopic observations suggested the presence of tail extensions of the well-known neutral sodium coma of Comets 1910I and Arend-Roland 1957III, the first clear images of a huge sodium tail  $10^7$  km long, well separated in the sky from classical dust and plasma tails, were obtained during the 1997 passage of Comet Hale-Bopp 1995O1 (Cremonese et al., 1997). The images were taken by means of interference filters centered on the sodium D lines at 589 nm, and the tail did not appear in simultaneous images taken on the  $H_2O^+$  line, showing a well-developed ion tail. The sodium tail appeared as a straight linear feature located between the ion tail and the prolonged radius vector. Simultaneous spectroscopic observations permitted measurement of the radial velocity of the neutral sodium atoms along the tail. The result was that a syndyne of  $\beta = 82$  best fit both the sodium tail axis orientation and the radial velocities along the tail. This was the first time that the  $\beta$  parameter was best constrained by means of radial velocity measurements. The sodium neutral atoms lighten because of fluorescence: Absorbed UV solar photons spend their energy to put the external sodium electrons in the most external orbitals. Since the solar photons are absorbed by the sodium atoms, their momentum is necessarily transferred to the sodium atoms, so that

$$\beta = \frac{hg(1 \text{ AU})^2}{\lambda GM_{\odot} m} \quad (19)$$

where  $h$  is the Planck constant,  $g$  the number of solar photons captured in the unit time by a sodium atom at 1 AU (or photon scattering efficiency in the sodium D lines),  $\lambda$  the wavelength of the sodium D lines, and  $m$  the tail particle mass. In perfect agreement with the theoretical com-

putations, the observed  $\beta = 82$  provides  $g = 15 \text{ s}^{-1}$  when we assume the atomic sodium mass for  $m$ . Therefore, the sodium tail is composed of sodium atoms and not of sodium molecules. The sodium atoms in space have a short lifetime, mainly due to photoionization. The sodium tail brightness along its axis  $x$  provides a unique measurement of the sodium lifetime  $\tau$ . Since the sodium tail axis can be best approximated by a syndyne, the whole sodium tail can be modeled by means of a syndynamic tube, whose photometric equation was computed by *Finson and Probst* (1968). When we consider the sodium lifetime against photoionization, the sky surface density of sodium atoms is

$$\delta(x,y) = \frac{\dot{N} \exp - \frac{t_0 - t(x)}{\tau}}{2v[t_0 - t(x)]w(x)} \quad (20)$$

where  $\dot{N}$  is the sodium loss rate,  $v$  the sodium ejection velocity (related to the sodium tail width),  $w$  the sodium radial velocity projected on the sky, and  $t$  the time of sodium ejection ( $w$  and  $t$  are provided by syndyne computations). Equation (20) perfectly fits the observed brightness on the tail axis  $x$  when we assume  $\tau = 1.7 \times 10^5 \text{ s}$  at 1 AU. This lifetime is three times larger than the value assumed in comet and planetary atmospheric models, as it was already suggested by laboratory measurements by *Huebner et al.* (1992).

## 8. CONCLUSIONS

Modeling the properties of the dust particles ejected from comets is one of the most formidable tasks in cometary physics, as we have little or no information about numerous parameters describing these dust grains. Quantities such as albedo, bulk density, radiation-scattering properties, shape, and grain spin are far from completely determined. There are other quantities either related to the dust sources dispersed on the nucleus surface or describing the dust-gas interaction in the coma, such as the dust velocity relative to the comet nucleus, the loss rate, and the particle size distribution, that are absolutely required by any realistic model that describes the dust environment of comets. It is impossible to obtain observational evidence that allows the inference of only one of these dust parameters. All of them are deeply interrelated, and only complex models that make use of all of them can provide a self-consistent scenario of the observations. For instance, it is usually assumed that the time evolution of the dust coma brightness allows us to deduce the time-dependent dust loss rate. However, the dust coma brightness depends on all the parameters listed above, and the loss rate is only one of them. Consequently, the interpretation of coma brightness in terms of the loss rate implicitly assumes that all the other dust parameters either play no role or have known values that do not change in time. All these assumptions are invalid.

Therefore, among complex models describing the motion of dust particles in comae and tails, one should pay most attention to the ones that contain the lowest possible

number of free parameters and that are able to provide the largest number of dust parameters after data fits have been obtained. Inverse dust tail models appear today as the most powerful tools we have to interpret groundbased (or Earth-orbiting satellite-based) data, because they only require assumptions on the dust grain shapes, their scattering efficiency, and albedo. Moreover, when thermal tail data are available, a comparison between outputs of tail models and optical coma photometry can provide an estimate of the average albedo of the dust. When high-quality data on both the IR and optical dust tails become available, inverse dust tail models will provide unique information on the temporal and grain-size dependencies of the dust albedo. Dust tail models predict the temporal evolution of the dust coma brightness, to be compared with the observations of the Afp parameter: This independent constraint allows one to establish that the dust environment deduced from modeling the IR and optical tail properties is indeed valid.

Information on the velocity imparted to the dust grains by the expanding gas is required to constrain three-dimensional model predictions for the gas dynamics in cometary comae; only dust tail models can provide estimates of the temporal and grain-size dependencies of the dust velocity. Information on the grain-size distribution is required by all models aimed at fitting the brightness of dust coma features. As a consequence, only inverse dust tail models can provide estimates of the time-dependent grain-size distribution. Cosmogonic and evolutionary models of comet nuclei require a good knowledge of the dust to gas ratio at the nucleus; only dust tail models can provide dust mass loss estimates that are not severely biased by assumptions of the related grain-size distribution. When high-quality data on all the parameters required to describe cometary dust grains become available, probably provided by future rendezvous missions to comets, complete and detailed models of the dust environment of comets will become possible. It is only then that one will be able to validly describe what space probes will face when meeting their targets. Only coordinated efforts among all modelers, taking into account the unique information that inverse tail models can provide, will enable the attainment of such an ambitious goal.

## REFERENCES

- A'Hearn M. F., Schleicher D. G., Feldman P. D., Millis R. L., and Thompson D. T. (1984) Comet Bowell 1980b. *Astron. J.*, *89*, 579–591.
- Burns J. A., Lamy P. L., and Soter S. (1979) Radiation forces on small particles in the solar system. *Icarus*, *40*, 1–48.
- Combi M. R. (1994) The fragmentation of dust in the innermost comae of comets: Possible evidence from ground-based images. *Astron. J.*, *108*, 304–312.
- Cremonese G., Boehnhardt H., Crovisier J., Rauer H., Fitzsimmons A., Fulle M., Licandro J., Pollacco D., Tozzi G. P., and West R. M. (1997) Neutral sodium from Comet Hale-Bopp: A third type of tail. *Astrophys. J. Lett.*, *490*, L199–L202.
- Crifo J. F. (1987) Are cometary dust mass loss rates deduced from optical emissions reliable? In *Interplanetary Matter* (Z. Ce-

- plecha and P. Pecina, eds.), pp. 59–66. Report G7, Czechoslovak Academy of Sciences, Ondrejov.
- Crifo J. F. (1991) Hydrodynamic models of the collisional coma. In *Comets in the Post-Halley Era* (R. L. Newburn Jr. et al., eds.), pp. 937–990. Kluwer, Dordrecht.
- Crifo J. F. (1995) A general physicochemical model of the inner coma of active comets. I. Implications of spatially distributed gas and dust production. *Astrophys. J.*, *445*, 470–488.
- Crifo J. F. and Rodionov A. V. (1999) Modelling the circumnuclear coma of comets: Objectives, methods and recent results. *Planet. Space Sci.*, *47*, 797–826.
- Dohnanyi J. S. (1972) Interplanetary objects in review: Statistics of their masses and dynamics. *Icarus*, *17*, 1–48.
- Epifani E., Colangeli L., Fulle M., Brucato J., Bussoletti E., de Sanctis C., Mennella V., Palomba E., Palumbo P., and Rotundi A. (2001) ISOCAM imaging of Comets 103P/Hartley 2 and 2P/Encke. *Icarus*, *149*, 339–350.
- Finson M. L. and Probst R. F. (1968) A theory of dust comets — I. Model and equations. *Astrophys. J.*, *154*, 327–352.
- Fulle M. (1987) A new approach to the Finson-Probst method of interpreting cometary dust tails. *Astron. Astrophys.*, *171*, 327–335.
- Fulle M. (1989) Evaluation of cometary dust parameters from numerical simulations: Comparison with analytical approach and role of anisotropic emission. *Astron. Astrophys.*, *217*, 283–297.
- Fulle M. (1990) Meteoroids from short-period comets. *Astron. Astrophys.*, *230*, 220–226.
- Fulle M. (1992) A dust tail model based on Maxwellian velocity distributions. *Astron. Astrophys.*, *265*, 817–824.
- Fulle M. (1999) Constraints on Comet 46P/Wirtanen dust parameters provided by in-situ and ground-based observations. *Planet. Space Sci.*, *47*, 827–837.
- Fulle M. (2000) The dust environment of Comet 46P/Wirtanen at perihelion: A period of decreasing activity? *Icarus*, *145*, 239–251.
- Fulle M. and Sedmak G. (1988) Photometrical analysis of the neck-line structure of Comet Bennett 1970II. *Icarus*, *74*, 383–398.
- Fulle M., Bosio S., Cremonese G., Cristaldi S., Liller W., and Pansecchi L. (1993) The dust environment of Comet Austin 1990V. *Astron. Astrophys.*, *272*, 634–650.
- Fulle M., Böhm C., Mengoli G., Muzzi F., Orlandi S., and Sette G. (1994) Current meteor production of Comet P/Swift-Tuttle. *Astron. Astrophys.*, *292*, 304–310.
- Fulle M., Mikuz H., and Bosio S. (1997) Dust environment of Comet Hyakutake 1996B2. *Astron. Astrophys.*, *324*, 1197–1205.
- Fulle M., Cremonese G., and Böhm C. (1998) The preperihelion dust environment of C/1995O1 Hale-Bopp from 13 to 4 AU. *Astron. J.*, *116*, 1470–1477.
- Fulle M., Lvasseur-Regourd A. C., McBride N., and Hadamcik E. (2000) In situ measurements from within the coma of 1P/Halley: First order approximation with a dust dynamical model. *Astron. J.*, *119*, 1968–1977.
- Greenberg J. M. and Li A. (1999) All comets are born equal: Infrared emission by dust as key to comet nucleus composition. *Planet. Space Sci.*, *47*, 787–795.
- Hanner M. S. (1984) A comparison of the dust properties in recent periodic comets. *Adv. Space Res.*, *4*, 189–196.
- Hanner M. S., Giese R. H., Weiss K., and Zerull R. (1981) On the definition of albedo and application to irregular particles. *Astron. Astrophys.*, *104*, 42–46.
- Harmon J. K., Campbell D. B., Hine A. A., Shapiro I. I., and Marsden B. G. (1989) Radar observations of Comet IRAS-Aracki-Alcock 1983d. *Astrophys. J.*, *338*, 1071–1093.
- Huebner W. F., Keady J. J., and Lyon S. P. (1992) Solar photo rates for planetary atmospheres and atmospheric pollutants — Photo rate coefficients and excess energies. *Astrophys. Space Sci.*, *195*, 1–7.
- Jewitt D. C. (1996) Debris from Comet P/Swift-Tuttle. *Astron. J.*, *111*, 1713–1717.
- Jewitt D. C. and Matthews H. E. (1997) Submillimeter continuum observations of Comet Hyakutake (1996B2). *Astron. J.*, *113*, 1145–1151.
- Kimura H. and Liu C. P. (1977) On the structure of cometary dust tails. *Chinese Astron.*, *1*, 235–264.
- Lvasseur-Regourd A. C., Hadamcik E., and Renard J. B. (1996) Evidence for two classes of comets from their polarimetric properties at large phase angles. *Astron. Astrophys.*, *313*, 327–333.
- Lvasseur-Regourd A. C., McBride N., Hadamcik E., and Fulle M. (1999) Similarities between in situ measurements of local dust light scattering and dust flux impact data in the coma of 1P/Halley. *Astron. Astrophys.*, *348*, 636–641.
- Lisse C. M. (2002) On the role of dust mass loss in the evolution of comets and dusty disk systems. *Earth Moon Planets*, *90*, 497–506.
- Lisse C. M., A'Hearn M. F., Hauser M. G., Kelsall T., Lien D. J., Moseley S. H., Reach W. T., and Silverberg R. F. (1998) Infrared observations of comets by COBE. *Astrophys. J.*, *496*, 971–991.
- Mason C. G., Gehrz R. D., Ney E. P., and Williams D. M. (1998) The temporal development of the pre-perihelion spectral energy distribution of Comet Hyakutake (C/1996B2). *Astrophys. J.*, *507*, 398–403.
- McDonnell J. A. M., Lamy P. L., and Pankiewicz G. S. (1991) Physical properties of cometary dust. In *Comets in the Post-Halley Era* (R. L. Newburn Jr. et al., eds.), pp. 1043–1073. Kluwer, Dordrecht.
- Pansecchi L., Fulle M., and Sedmak G. (1987) The nature of two anomalous structures observed in the dust tail of Comet Bennett 1970II: A possible neck-line structure. *Astron. Astrophys.*, *176*, 358–366.
- Sekanina Z. (1988) Outgassing asymmetry of periodic Comet Encke. I. Apparitions 1924–1984. *Astron. J.*, *95*, 911–924.
- Sekanina Z. and Schuster H. E. (1978) Meteoroids from periodic Comet d'Arrest. *Astron. Astrophys.*, *65*, 29–35.
- Sekanina Z. and Farrell J. A. (1980) The striated dust tail of Comet West 1976VI as a particle fragmentation phenomenon. *Astron. J.*, *85*, 1538–1554.
- Waniak W. (1992) A Monte-Carlo approach to the analysis of the dust tail of Comet 1P/Halley. *Icarus*, *100*, 154–161.
- Waniak W. (1994) Nuclear dust emission pattern of Comet Wilson 1987VII. *Icarus*, *111*, 237–245.

